Optimal setting of bendable optics based on FEA calculations

Nikolay A. Artemiev,[a*] Ken P. Chow,[a] Daniele La Civita,[b] Daniel J. Merthe,[a] Yi-De Chuang,[a] Wayne R. McKinney,[a] and Valeriy V. Yashchuk[a]

[a] Advanced Light Source, Lawrence Berkeley National Laboratory, 1 Cyclotron Road, Berkeley, CA 94720, USA;

[b] European XFEL, Albert-Einstein-Ring 19, 22765 Hamburg, Germany

ABSTRACT

Recently, a technique for optimal tuning and calibration of bendable x-ray optics using surface slope data obtained with a slope measuring long trace profiler (LTP) was developed at the Advanced Light Source (ALS) optical metrology laboratory (OML) [Opt. Eng. 48(8), 083601 (2009)]. In this technique, slope distributions measured at different settings of the bending couples at each end of a flat substrate are used to construct bender characteristic functions. Using regression analysis with the experimental characteristic functions, optimal settings of the benders that best approximate the desired shape in slope are determined. In this work, we describe a method for finding a bender's characteristic functions based on Finite Element Analysis (FEA) of a complete mirror assembly. The accuracy of the characteristic functions found by simulation is verified by cross comparison with experimental characteristic functions for a long (450 mm) highly curved bendable mirror. The mirror has a sagittally shaped substrate developed for the ALS MERLIN beamline 4.3.0, with a total slope variation 15 mrad. Calculating FEA characteristic functions in the design stage allowed better understanding of the design of the bender's adjustment mechanism. By calculating FEA characteristic functions a priori, we significantly decrease the time needed in the OML for tuning the mirror. Because the calculated characteristic functions are free of the errors inherent to measurements made in the lab, the tuning is even more accurate.

Keywords: x-ray optics, Kirkpatrick-Baez, bendable mirrors, characteristic function, regression analysis, long trace profiler, metrology of x-ray optics, Finite Element Analysis, FEA.

1. INTRODUCTION

Synchrotron radiation sources of third- and fourth-generation deliver X-ray beams of extremely high brilliance, demanding unprecedented quality of X-ray optics to preserve the beam coherency and brightness. Corresponding figure errors of such optics should be of the order of 0.1 - 0.2 μrad rms [1-4]. One of the most effective, simple, and widely used methods of achieving ultra-fine focusing is the use of a Kirkpatrick-Baez pair of mirrors [5]. This method uses a pair of orthogonally arranged mirrors having the shapes of elliptical cylinders. These mirrors focus an X-ray beam in the sagittal and meridional directions separately. Achievements in manufacturing of figured surfaces allow for using mirrors with figures of rotation like ellipsoids and paraboloids [6-8]. However, cost of such optical elements is prohibitive in many cases. Flat optics are cheaper, much easier to manufacture and more accurately measured.

To control the shape of an initially plane optic, bending torques (or couples) are applied to the edges of the substrate [9]. In order to bend such an optic to a desired shape with a high degree of accuracy, the substrate is shaped sagittally [10], where we extended [11]. Moreover, it is often difficult to measure all and adjust parameters of the optical scheme of an existing beamline with a sufficient level of accuracy. Bendable optics allow fine adjustment of their shapes right at the beamline that let them to adopt the existing parameters of the optical scheme or even refocus for different distances. Tuning of a figured optic can be a more complicated process because the shape of the optic is fixed and fine focusing is achieved by mutual adjustment of all optical components of the beamline.

*NArtemiev@lbl.gov; phone 1 510 495-2159; fax 1 510 495-2719; http://opticalmetrology.lbl.gov

To fine tune bendable optics, we utilize a method of characteristic functions described in [12, 13], which was initially developed for adjustment of mirrors on synchrotron radiation beamlines [14]. Surface slope data obtained with a slope measuring profiler [15, 16] in the optical metrology laboratory (OML) of the Advanced Light Source (ALS) is used in this method for optimal tuning of bendable optics. Making use of inherent linearity of the problem, only three slope profiles measured consecutively before and after small adjustments of each bending couple are needed. Two characteristic functions, one for each bender, are calculated on the base of the measured slope traces.

Knowledge of the characteristic functions of the system is of vital importance not only for setting the shape of an optic in the metrology lab, but also for fine tuning the optic in situ at the beamline [21]. When installing the optic at a beamline various factors may affect the optic's shape that was initially preset in the OML. The following factors may considerably spoil the focusing properties of the optic like changes of ambient temperature, almost unavoidable shakes during transportation of the system from the metrology lab to the beamline and installation the optic in its working place, evacuating the mirror tank, increase (or temporal variation) of the optic's substrate temperature due to synchrotron radiation heat load, etc. But the most important is accuracy of the optic's alignment with respect to the other beamline optics and precision of measurements of the actual mutual arrangement of the beamline optical elements. The ability to achieve a fast and accurate tuning of the mirror slope plays a crucial role in the beamline performance as a whole.

Systematic errors, instrumental drifts, and manufacturing imperfections of the optic's surface finish considerably limit the accuracy of measurement of characteristic functions. On the other hand the shape of a bendable optic calculated by finite element analysis (FEA) is free of all kinds of intrinsic experimental errors, rather than possible errors of modeling. As soon as each bendable optic is designed with the help of FEA, we can try to make use of it and calculate the characteristic functions right at the design stage. A single FEA calculation of a bendable optic's shape takes tens of minutes or an hour in the most complicated case, while experimental measurements of a single slope trace may last more than a working day.

In this work we report a method of calculation of characteristic functions by means of FEA and compare the application of FEA-calculated and experimentally measured characteristic functions for tuning of the finite element model of the mirror and the actual hardware to a desired shape. We describe how the actual mirror can be tuned to the desired shape with the same level of accuracy using of either set of the characteristic functions, while saving days of painstaking slope trace metrology. We demonstrate that the finite element model can be tuned to the ideal desired elliptical cylinder with the accuracy of approximately 30 nrad. Finally we discuss the difference in shapes of the calculated and measured characteristic functions and show that it influences only the numerical coefficients resulting from the regression analysis and does not affect the accuracy of the mirror setting.

A model of the mirror assembled with a bending mechanism that applies two couples at the substrate's ends is shown in Fig. 1. The flat substrate's overall dimensions are approximately 450 x 20 x 7 mm^3. In order to achieve a best approximation to a tangential ellipse the substrate has shaped sides as shown in Fig. 2 [10].

The length of the clear aperture of the mirror is 340 mm symmetrically arranged around the geometrical center of the substrate. In the tangential direction the substrate is to be bent to an ellipse with the following parameters: the source - to - mirror distance r = 3895.12 mm, the mirror - to - focus distance r' = 1000.00 mm, and grazing incidence angle θ = 3.0 deg. According to the above mentioned parameters, the mirror has a slope variation of 11.2 mrad within its clear aperture. This value is considerably larger than the OML Long Trace Profiler LTP-II's measuring range, which is 5 mrad [16]. This way one slope measurement must consist of at least three consecutive measurements along the surface under test (SUT) made with reasonable overlapping for necessary stitching.

FEA simulations for two different cases of boundary conditions applied to the leaf springs are considered. In the first case, forces are applied to the bender's leaf springs as boundary conditions. This case is used when designing the mirror benders. In the second case, displacements of the benders' leaf springs are applied to the finite element model as the boundary conditions. This case more accurately models the mirror assembly, and can be compared with the results of the measurement in the OML.

2. THE OPTIC UNDER CONSIDERATION AND ITS FEA MODEL

We describe the advantages of the method using the example of bendable mirror M323 [17] of the ALS beamline BL4.0.3 MERLIN [18].

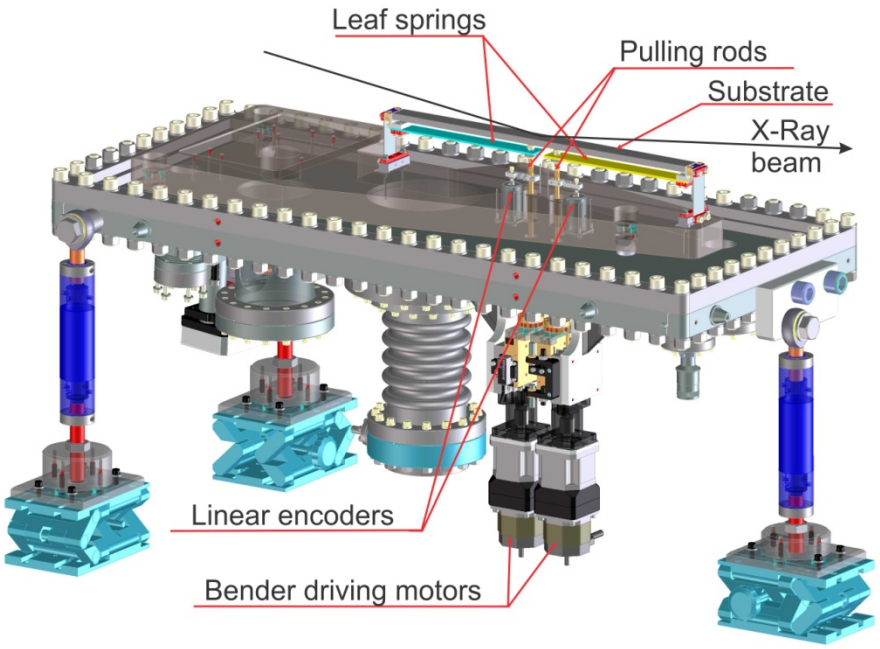

Figure 1: A model of bendable mirror M323 for the ALS beamline BL4.0.3 MERLIN with a leaf spring-based bending mechanism. The mirror is shown in a tripod adjustable support prepared for measurements and setting with the OML long trace profiler.

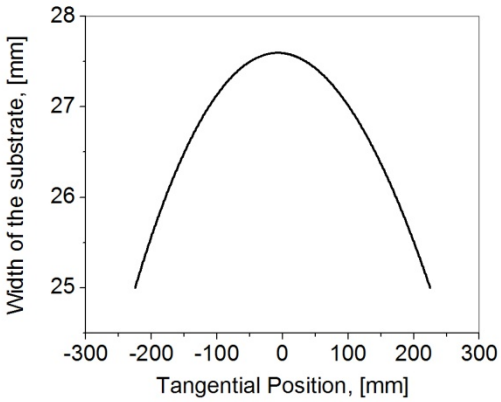

Figure 2: The width of the mirror substrate as a function of the tangential position.

The finite element model of the mirror was developed using ANSYS® Workbench™ [19]. Only half of the full assembly is modeled to take advantage of symmetry conditions. The model is comprised of 179,000 tetrahedral and hexahedral second-order elements, with a 1.5 mm element size in the body of the optic, a 1 mm element size in the end blocks, 3 elements

across spring thicknesses, and a 0.4 mm element size at the glued interface between the optic and end blocks. Fixed face boundary conditions are applied at the bottom faces of the side spring mounting blocks. Load and boundary conditions are applied to the leaf springs either as remote displacements or remote forces at the centers of the leaf springs' pull-rod holes. All interfaces between different materials are modeled as bonded interfaces. The thin glue joints between mirror and end blocks are not included in the model.

3. FORCE-BASED AND DISPLACEMENT-BASED BOUNDARY CONDITIONS

In many cases in FEA calculations, it is more common to apply forces instead of displacements as boundary conditions. From the point of view of calculation of performance of a bendable optic there is not too much difference. By applying forces, an engineer calculates the reaction of the system and studies the behavior of its parts. The most important parameters are the dynamic range of the displacements of the elements that apply the couples, typically leaf springs, and forces needed to be applied to these elements in order to achieve a desirable shape of bendable optic. However, later on when the bender is assembled and ready to work, displacements not forces are applied to the springs. At this step one uses Linear Variable Differential Transformers (LVDTs) [20] to measure the positions of the springs and interpret this information to judge the bendable optic's shape and slope. The reason for this lies in construction of the bender, not in a priori bias of the metrologist or the beamline scientist.

Use of forces as boundary conditions complicates the analysis because the corresponding displacements are extracted from the FEA as secondary calculated parameters, while in most of practical designs the displacements are used as the parameters measured in the course of setting the mirror shape and slope. The benders' reactions are different depending whether forces or displacements are applied as boundary conditions.

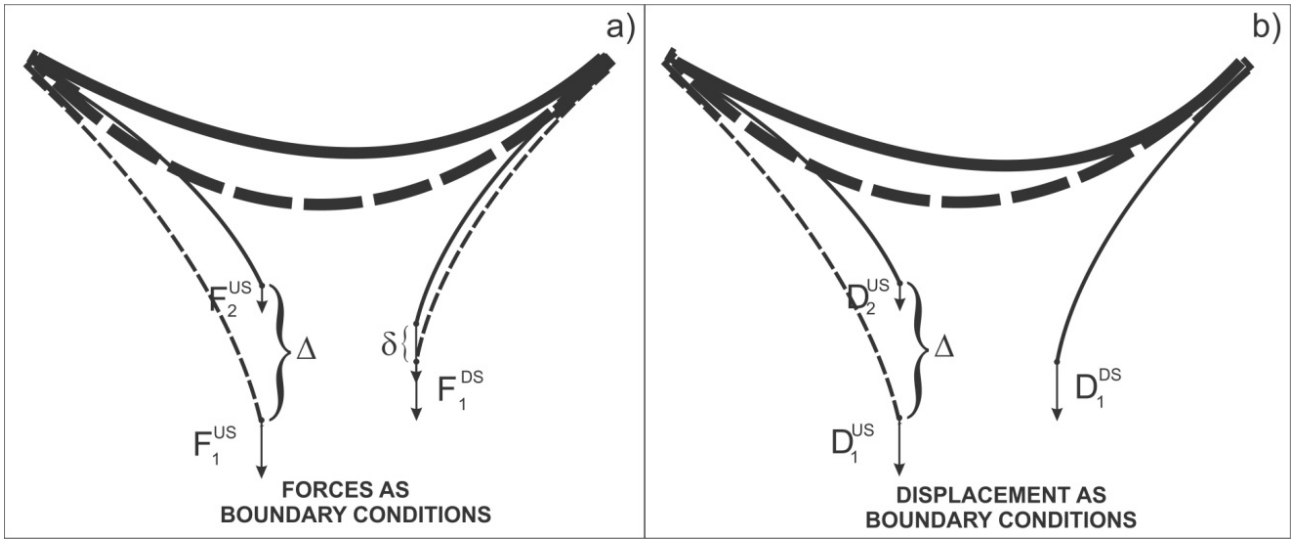

Figure 3: Schematics of application of forces (left image) and displacements (right image) as boundary conditions. In both cases the position of the left leaf spring was changed. Dashed lines show initial positions of the elements, while solid lines represent positions of the elements after tuning.

Due to cross talk between the upstream and downstream benders via change of the substrate's stress, the application of a force to one leaf spring leads to a position change of the other one, while the corresponding force is not appropriately compensated. Such a behavior of the bender mechanism is in contradiction to the actual hardware. This situation is depicted in Fig. 3 a). Decreasing of force F1 applied to the left leaf spring leads to change the position of the right leaf spring.

In a more common design, setting of the bender is made by changing the position of the corresponding leaf-spring's end. The position of the other spring is unchanged (see Fig. 2 b). In such design change of settings of the benders is done independently one from the other and the crosstalk between the benders does not lead to interplay between the springs' positions.

Using FEA, we calculate surface heights and slope distributions of a bent substrate before and after single small adjustments of each bending couple by changing corresponding boundary conditions. In this way the characteristic functions of a bendable optic calculated by FEA made for the case of force-based boundary conditions may not be readily applied to the designed benders that use displacement-based boundary conditions.

4. CALCULATION OF CHARACTERISTIC FUNCTIONS FROM FEA

As shown in Ref.,[12] slope variation of a bent substrate can be expressed as a linear combination of two functions as follows:

$$\alpha(x,C) = C_1 f_1(x) + C_2 f_2(x), \tag{1}$$

where x is tangential coordinate along the substrate, $f_1(x)$ and $f_2(x)$ are characteristic functions specific for the mirror design, and the constants C_1 and C_2 are the bending couples applied to the bendable mirror.

In order to get characteristic functions, it is needed to perform three slope calculations with different constants C_1 and C_2:

$$\alpha_1(x,C) = C_1 f_1(x) + C_2 f_2(x) \tag{2}$$

$$\alpha_2(x,C) = (C_1 + \Delta C_1) f_1(x) + C_2 f_2(x) \tag{3}$$

$$\alpha_3(x,C) = C_1 f_1(x) + (C_2 + \Delta C_2) f_2(x), \tag{4}$$

where α_1 is the slope profile of the substrate that corresponds to the designed values of boundary conditions, α_2 and α_3 are slope profiles calculated for relatively small changes of the couples applied to the upstream and downstream benders. Solving the system of equations (2-4) we obtain:

$$f^*_1(x) = \frac{\alpha_2(x) - \alpha_1(x)}{\Delta C_1} \tag{5}$$

$$f^*_2(x) = \frac{\alpha_3(x) - \alpha_1(x)}{\Delta C_2}. \tag{6}$$

The asterisk denotes that these are estimated values of the functions contrary to the true value in the previous equations. The most accurate solution is acquired in a vicinity of a working point of the system, i.e. when positions of the benders correspond to the desired (closest to the desired) shape of the substrate.

In the design, shown in Fig. 1 the bending couples are proportional to the applied displacements or forces, applied to the leaf springs (see Fig. 3) as boundary condition used for FEA simulations. This allows one to numerically calculate characteristic functions of the benders in terms of used boundary conditions. An initial substrate slope profile $\alpha 1$ and positions of the leaf springs D_1^{US} and D_1^{DS} for designed values of the forces F_1^{US} and F_1^{DS} applied as boundary conditions to the upstream and the downstream leaf springs respectively is calculated for designed values of the boundary conditions. The superscripts US and DS indicate upstream and downstream parts of the mirror.

In order to calculate characteristic functions in the case of using forces as boundary conditions, first, we change the force applied to the upstream bender leaf spring by 1% and keep the force applied to the downstream bender leaf spring at its design value. As a result of the consequent FEA calculation we obtain the new position of the upstream leaf spring D_2^{US} and

the slope profile α_2^F of the substrate; second, we change the force applied to the downstream bender leaf spring by 1% and keep the force of the upstream bender leaf spring at its design value. As a result of the consequent FEA calculation we obtain the new position of the downstream leaf spring D_2^{DS} and the slope profile α_3^F of the substrate. Corresponding force-based characteristic functions will have a form (see Fig. 2):

$$f_1^F(x) = \frac{\alpha_2^F(x) - \alpha_1(x)}{D_2^{US} - D_1^{US}} \tag{7}$$

$$f_2^F(x) = \frac{\alpha_3^F(x) - \alpha_1(x)}{D_2^{DS} - D_1^{DS}}, \tag{8}$$

where the superscript "F" stands for force-based boundary conditions.

In the case of using displacements as boundary conditions to calculate the slope profile α_2^D we set the position of the upstream leaf spring to D_2^{US}, but at the same time the downstream leaf spring is kept at its designed position D_1^{US}. To calculate the slope profile α_3^D we set the position of the upstream leaf spring to D_2^{DS} and the upstream leaf spring is kept at its designed position. Corresponding displacement-based characteristic functions will have a form (see Fig. 2):

$$f_1^D(x) = \frac{\alpha_2^D(x) - \alpha_1(x)}{D_2^{US} - D_1^{US}} \tag{9}$$

$$f_2^D(x) = \frac{\alpha_3^D(x) - \alpha_1(x)}{D_2^{DS} - D_1^{DS}}, \tag{10}$$

where the superscript "D" stands for displacement-based boundary conditions.

Characteristic functions calculated by FEA, when forces or displacements were used as boundary conditions applied to the leaf springs are shown in Fig. 4a. The characteristic functions calculated for the two cases of boundary conditions differ by approximately 4% rms over the clear aperture. The reason is the difference in reaction of one leaf spring on a change of position of the other one for the two cases of boundary conditions used in corresponding FEA calculations. This difference is of the same order of magnitude as the difference in displacements of the leaf springs when forces or displacements were used as boundary conditions.

As seen in Fig. 4b, the difference between characteristic functions computed by the FEA for the two cases of boundary conditions is as small as ± 10 nrad/μm at the extremities of the clear aperture. Such a difference is not noticeable when correcting the mirror's shape in a vicinity of its working point. However, the absolute values of the leaf spring displacements needed to bend the mirror starting from an initially flat shape are of the order of 10,000 μm. Performing a prediction on the basis of characteristic functions calculated for the case of boundary conditions, which do not correspond to the designed and manufactured optic, starting right from the initially flat mirror will bring unacceptable slope errors as large as 0.2 mrad over the entire clear aperture.

To check the linearity of the finite element model we performed two sets of FEA calculations of the characteristic functions. The first set of calculations was made for 1% variations of the leaf spring displacements. Such a small variation of the leaf spring displacements is used routinely in the OML for measuring characteristic functions of bendable optics. The second set of calculations of the characteristic functions was made with 10% variations of the leaf spring displacements. Comparison of the two sets of the characteristic functions revealed no noticeable difference between the functions. The difference between the characteristic functions is on the level of 15 prad/μm rms. This corresponds to the inaccuracy of the FEA calculations and

consequent post-processing of the FEA results obtained for 1% variations of the leaf spring displacements. Comparing this result with the entire range of the characteristic functions, 370 nrad / μm for the upstream and 470 nrad / μm and for the downstream benders, we can conclude that the finite element model of the mirror can be considered as linear with an accuracy of better than 10^{-4}.

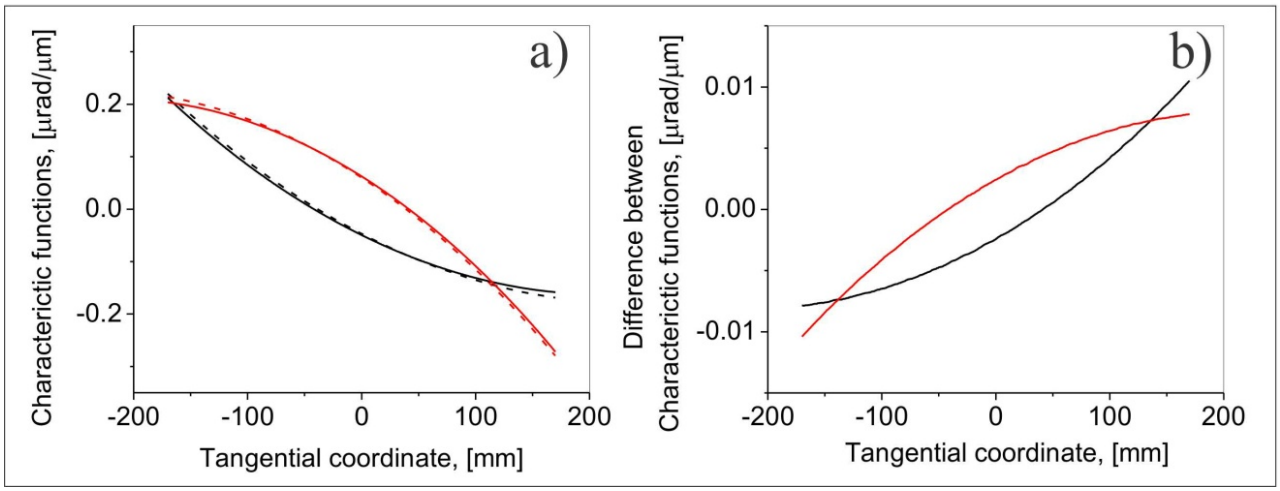

Figure 4: a) Characteristic functions calculated by FEA when forces (dashed curves) or displacements (solid curves) were used as boundary conditions. b) Difference between the upstream (black lower curve) and downstream (red upper curve) characteristic functions calculated for the cases when displacements or forces boundary conditions were applied to the leaf springs.

Application of boundary conditions with designed values of forces or displacements does not lead to the best possible shape of the substrate's finite element model. However, we may try setting the finite element model of the substrate as close as possible to its desired shape using the calculated characteristic functions.

A slope difference between the ideal desired shape and the shape predicted by the method of characteristic functions (see Ref.[12]) of the substrate's finite element model is shown in Fig. 5. The tangential profile of the substrate resulting from the FEA calculated for the designed bender parameters optimized by the method of characteristic functions is as close to the desired slope as 32 nrad rms. In this case the characteristic functions are calculated from the FEA results, when displacement variations are applied as boundary conditions. Apparently this is the best possible approximation to the ideal elliptical slope for these benders and the designed sagittal shape of the mirror's substrate (see Fig. 2).

The curve in Fig. 5 exhibits two kinds of variations. The low spatial frequency variation with an amplitude ± 50 nrad could be related to the finite accuracy of the substrate shaping in the sagittal direction. The high spatial frequency irregularity on the order of 1 to 2 nrad is likely related to the limited accuracy of the FEA calculations and consequent post-processing of the results.

It is worth noting that the third order polynomial variation of the residual slope appears in the height domain as a fourth order polynomial, the so-called bird-like profile. Such a bird-like shape relates to a non-zero Poisson ratio of the material of the substrate. By bending a beam, we contract material in its inner part while stretch material in outer part. This leads to the effect that on both ends of the beam material tends to unbend the beam and appears as bird-like shape in the residual after subtracting ideal (elliptical, cylindrical, or parabolic second order profile) shapes. This effect is not taken into account in thin beam theory upon which calculation of sagittal shaping the substrate's sides were performed.

As a consistency check the exact elliptical slope distribution to which the finite element model is tuned by the method of characteristic functions was calculated with IDL™, MathCad™, and Delphi™ software independently. The difference between any two of these slope distributions is of the order of 10^{-15} rad rms.

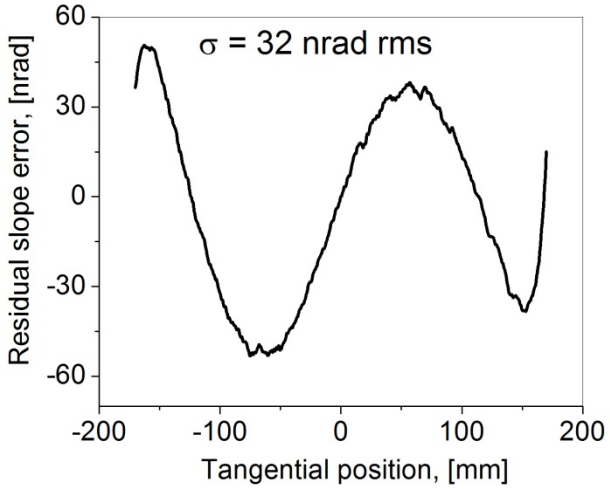

Figure 5: Slope difference between the ideal desired and predicted by the method of characteristic functions (see Ref.[11]) slope profiles of the substrate's finite element model.

In the approximation of linear response of the system to small changes of boundary conditions, we can construct the characteristic functions for the case of force-based boundary conditions knowing only the characteristic functions calculated for displacement-based boundary conditions. Indeed, the upstream and downstream bender characteristic functions for the case of force-based boundary conditions can be presented as a superposition of the upstream bender characteristic function and the downstream bender characteristic function calculated for the case when displacements were used as boundary conditions:

$$\begin{aligned} f_F^{US} &= f_D^{US} + k1 \cdot f_D^{DS} \\ f_F^{DS} &= f_D^{DS} + k2 \cdot f_D^{US} \end{aligned} \tag{11}$$

where subscripts "F" and "D" denote the cases when forces or displacements were used as boundary conditions; and superscripts "US" and "DS" show to which bender, i.e. the upstream and the downstream, the characteristic function belongs.

Each coefficient in equations (11) is the ratio of the relative changes of displacements of a reactive and active leaf spring calculated for the force-based boundary conditions (Table 1).

Solving this system of equations we can calculate the characteristic functions for displacement-based boundary conditions knowing only the characteristic functions calculated for force-based boundary conditions, and the coefficients calculated as a ratio of values of displacements of the leaf springs of reactive and active benders.

$$\begin{aligned} f_D^{US} &= \frac{f_F^{US} - k1 \cdot f_F^{DS}}{1 - k1 \cdot k2} \\ f_D^{DS} &= \frac{f_F^{DS} - k2 \cdot f_F^{US}}{1 - k1 \cdot k2}. \end{aligned} \tag{12}$$

The curves in Fig. 6 show the differences between FEA calculated characteristic functions for the case when displacements were used as boundary conditions, and the functions calculated from the Eqs. (12). Plots a) and b) show the results for 1% and 10% variations of boundary conditions respectively.

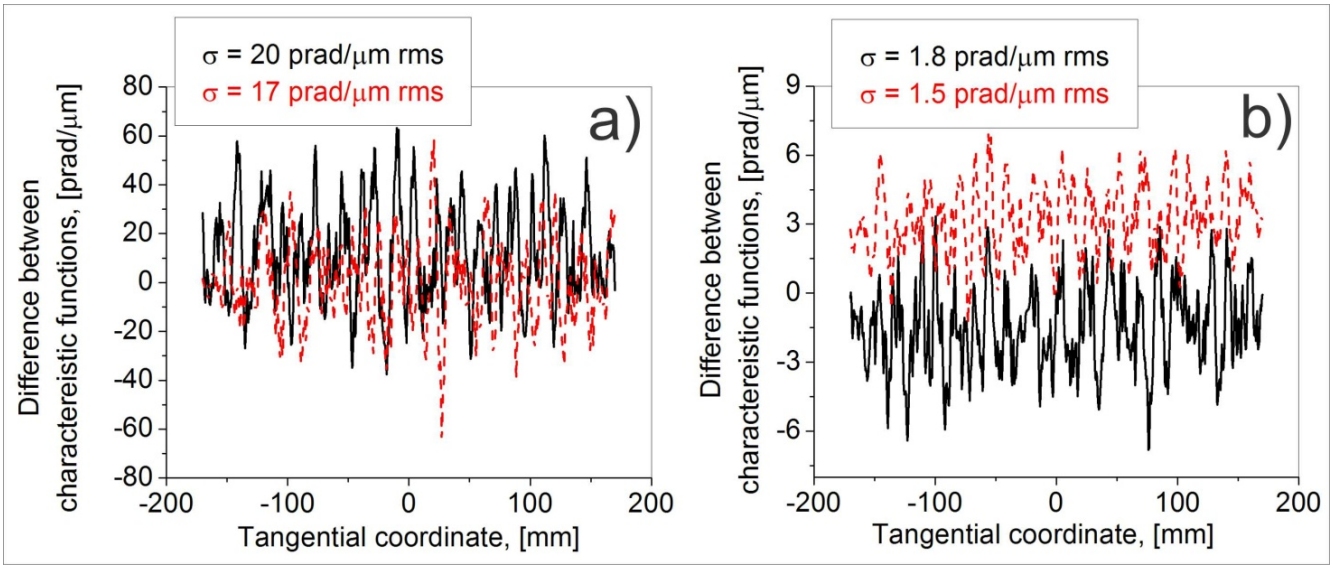

Figure 6: The differences between FEA calculated characteristic functions for displacement-based boundary conditions, and the functions calculated from Eqs. (12) computed for a) 1% variation of boundary conditions, and b) 10% variation of boundary conditions. Black solid curves correspond to the upstream bender; red dashed curves correspond to the downstream bender.

The differences between characteristic functions calculated by Eqs. (12) and the FEA calculated ones for 1% variation of the leaf springs displacements are 20 prad/ μm rms and 17 prad/ μm rms (Fig. 6 a) for the upstream and the downstream benders respectively. The precision of these calculations is limited by the accuracy of the FEA calculations and the consequent post-processing of the FEA results. Precisely calculated characteristic functions allow setting the substrate to the desired shape as close as 0.2 μrad starting right from the initially flat shape of the substrate. And as soon as the final setting of a bendable optic is normally started from the initially pre-bent position, which is close to the desired one, the first iteration may already give desired accuracy of the shape of the optic.

Due to ten times increase of the denominator in Eqs. (9) and (10) the ten times larger variations of the leaf springs displacements result in approximately ten times lower noise amplitude in the characteristic function differences (see Fig. 6 b).

5. MEASUREMENT OF CHARACTERISTIC FUNCTIONS AND SETTING THE OPTIC IN THE OML

Fig. 7 shows the experimental arrangement of LTP-II slope measurements with bendable mirror M323 of the ALS beamline 4.0.3. MERLIN. The mirror base plate was lifted up above the surface of the optical table by approximately 70 cm to allow enough space for allocation of the driving motors with vacuum feedthrough of the benders' pulling rods. Therefore, the LTP-II ceramic beam was placed at a nearly highest possible position that corresponds to approximately 1 m vertical distance between the optical table and the lowest point of the LTP optical sensor. To provide angular adjustment of the SUT with respect of the LTP-II the mirror was placed on a three point support rested on three vertical jacks.

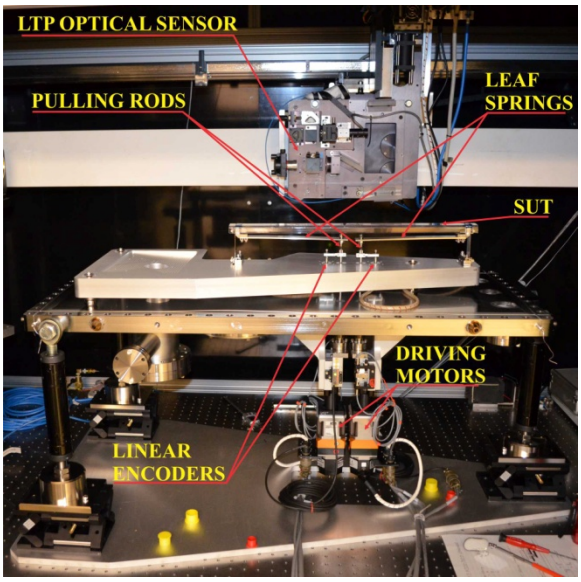

Figure 7: Experimental arrangements of the LTP-II measurements with bendable mirror M323 [17] of ALS beamline 4.0.3 MERLIN [18].

The SUT's slope variation was 11.2 mrad within the clear aperture, while the working range of the LTP-II is only 5 mrad. It necessitated angular realignment of the SUT during the measurements. The angular realignment was realized by lifting and lowering one vertical jack shown in the right hand side of Fig. 7. The SUT slope trace measurements consisted of five overlap regions schematically shown in Fig. 8. Tangential lengths, corresponding total slope variations of the measurement regions, as well as the tilt angles of the SUT between the measurements are indicated in Table 1.

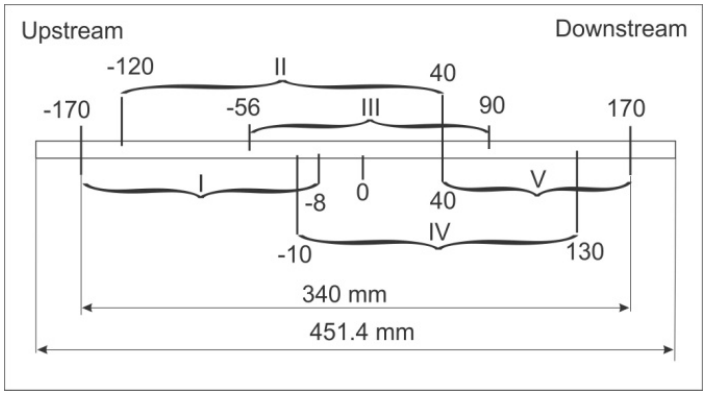

Figure 8: Schematic of the mirror's substrate with indication of the five overlapping regions of measurement.

The measurement of the mirror was made in two steps. At the first step we measured the characteristic functions and set the mirror to the desired elliptical shape. To save time during these measurements the SUT was measured over the three ranges that correspond to regions I, III, and V in Fig. 8 and Table 1. The mirror has been tilted between each slope trace measurement. Each region was measured with a step of 2 mm. In order to suppress instrumental linear drift error, each slope

trace measurement consisted of two scans performed in forward and backward scanning directions according to an optimal scanning strategy (see Refs.[14, 20]).

Table 1: Tangential lengths and total slope variation of the measurement regions.

Measurement region	I	II	III	IV	V
Length	162 mm	160 mm	146 mm	140 mm	130 mm
Total slope variation	4860.3 μrad	5045.9 μrad	4900.0 μrad	4942.5 μrad	4853.4 μrad
Tilt angle for 3 ranges	3353 μrad		3104 μrad		
Tilt angle for 5 ranges	1507 μrad	1848 μrad	1477 μrad	1628 μrad	

Unfortunately, the axis of rotation of the tilt did not coincide with geometrical center of the SUT and that introduced a tangential shift of the mirror between different angular positions of the mirror with respect to the LTP translation system. To control this shift an electronic measuring head was installed at the upstream side of the mirror. It measured the absolute tangential shift of the aluminum base plate of the mirror's substrate. Because of the difference in heights of the aluminum base plate and the SUT above the unknown location of the rotation axis the actual shift of the SUT was measured with the LTP optical sensor once for each tilt. Accuracy of measurement of the tangential positioning of the SUT is estimated to be not greater than 0.01 mm. The readings of the electronic measuring head were tabulated and used every time for correction of the LTP optical sensor position when changing the ranges of the measurements.

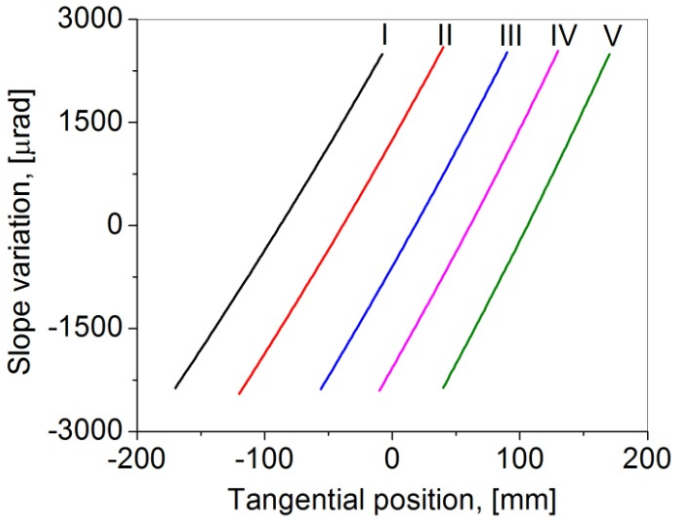

Figure 9: Piecewise slope profiles of the SUT measured over the regions shown in Fig. 8. Serial number of the region is indicated above every curve.

In order to obtain the full slope profile over the whole clear aperture from the piecewise discontinuous slope profiles shown in Fig. 9 we apply the following stitching procedure.

In each overlap region we find the average of each pair of functions. For example, between coordinates -120 mm and -8 mm (see Fig. 8) we average curve pair I and II respectively. Next we add this average to curve set I, and subtract it from curve set

II. At this step we obtain a stitched curve for regions I and II. The procedure is then applied to the overlap region between the I-II stitched curve and curve III and so on. Finally, piston is removed such that for the full slope profile the center value is (0,0).

Constructing three slope profiles corresponding to ±200 μm adjustments of the upstream and the downstream benders the characteristic functions could be calculated in accordance with Eqs. (5) and (6). However, in this case systematic errors of the measuring instrument and errors related to non-ideal repositioning of the LTP optical sensor with respect to the measurement regions of the SUT may noticeably influence the accuracy of stitching of the slope profiles. As a consequence, the resulting characteristic functions may be distorted and that would lead to lower precision of predictions of the benders' settings, increasing the number of iterations and, finally to less accurate setting the mirror to the desired shape.

On the contrary, we can make use of the differential nature of the characteristic functions, calculating them separately for each region of measurements and subsequently stitching them together. In this case, the slope profiles measured over the same region but for different sets of the benders' settings contain almost exactly the same systematic errors of the measuring instrument. A partial characteristic function calculated for each particular measurement region is not sensitive to the systematic errors due to the fact that subtracting very similar slope profiles will effectively cancel out the systematic errors which belong to this particular position of the LTP optical sensor and this particular optical path of the probe beam through the LTP optics.

This way the characteristic functions of the mirror were calculated separately for each of the three ranges of measurements. Parts of the characteristic functions measured over each of three measurement range are shown in Fig. 9.

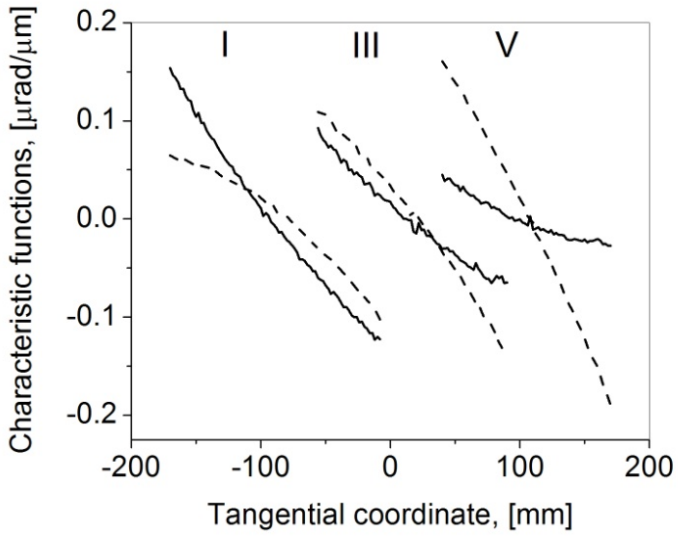

Figure 10: Piecewise characteristic functions measured over each individual measurement range. Solid and dashed curves show parts of the upstream and downstream benders' characteristic functions respectively.

In order to synthesize a single set of characteristic functions from the piecewise discontinuous functions shown in Fig. 10 we apply exactly the same procedure as if we were stitching slope data. These discontinuities are, of course, due to the fact that the slope range of the SUT is greater than that of the LTP.

In each overlap region we find the average of each pair of functions. For example, between coordinates -56 mm and -8 mm (see Fig. 8) we average curves pair I and III respectively. Next we add this average to curve set I, and subtract it from curve

set III. At this step we obtain a stitched curve for regions I and III. The procedure is then applied to the overlap region between the I-III stitched curve and curve V. Finally, piston is removed such that for each function the center value is (0,0).

To estimate the influence of possible inaccuracy of repositioning the LTP optical sensor over each measurement range we approximate the SUT's slope profile with a linear function:

$$S = 0.033\frac{rad}{m} \cdot x \tag{13}$$

Taking into account the precision of superimposing of adjacent measured regions as 0.01 mm we obtain an accuracy of stitching equal to 0.33 μrad. This value is on the level of accuracy of LTP-II slope measurements of highly curved optics.

At the second step the mirror was measured over 5 ranges (see Fig. 8 and Table 1) with a step of 2 mm along the clear aperture in exactly the same manner as during measurement of characteristic functions. This provided a larger overlap between the measured regions and consequently, better accuracy of stitching. The total measurement time of the full clear aperture was approximately 3 h and 40 min including the mirror tilting and the consequent check of the SUT alignment with respect to the LTP optical sensor.

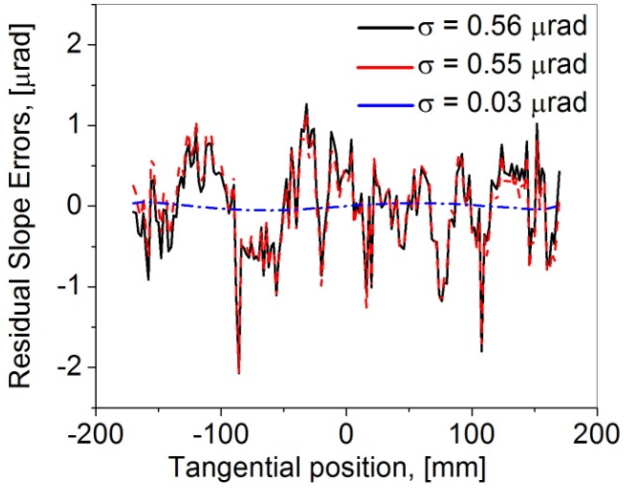

Figure 11: Residual after subtraction of the desired elliptical slope traces of the mirror. The black solid curve shows the residual of the experimentally measured mirror's slope profile tuned by experimentally measured characteristic functions. The red dashed curve shows the residual of the slope profile of the actual substrate predicted with the FEA calculated with displacement-based characteristic functions. The blue dash-dotted curve shows the residual of the slope profile of the finite element model of the mirror tuned by the same FEA-calculated characteristic functions.

The residuals after subtraction of the desired elliptical slope profile are shown in Fig. 11. The black solid curve shows the residual of the experimentally measured mirror's slope profile tuned by experimentally measured characteristic functions. The red dashed curve shows the residual of the slope profile of the actual substrate predicted with the FEA-calculated displacement-based characteristic functions. The rms slope variations in both cases are almost exactly the same and equal to 0.56 mrad for the experimentally measured slope profile and 0.55 for predicted slope profile of the actual mirror on the base of the FEA calculated characteristic functions. To compare the resulting experimental slope profile of the actual mirror with the best possible achievable profile for the actual shape of the substrate, the blue curve in Fig. 11 represents the residual after

subtraction of the ideal desired elliptical slope profile from that of the finite element model of the substrate shown earlier in Fig. 5.

6. COMPARISON OF FEA AND EXPERIMENTAL RESULTS

Characteristic functions measured experimentally on the actual hardware and calculated from the FEA results are shown in Fig. 12 a).

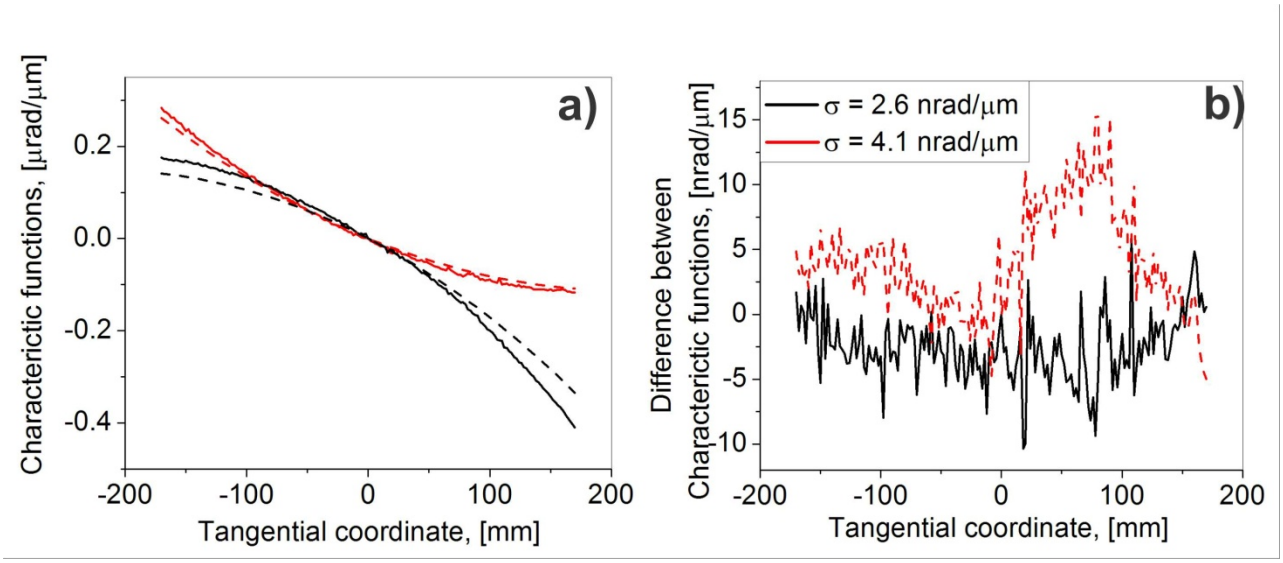

Figure 12: a) Experimentally measured (solid curves) and FEA calculated (dashed curves) characteristic functions. b) Difference between experimentally measured and corrected FEA-calculated characteristic functions: upstream (solid curve) and downstream (dashed curve). Black and red curves show upstream and downstream characteristic functions respectively.

The characteristic functions shown in Fig. 12 a) calculated by FEA are a little bit less steep than the measured ones. This discrepancy is related to a not exact correspondence of the finite element model to the physical realization of the system. Material constants and actual dimensions of the system's components may vary within tolerances. However, the main advantage of the characteristic function method is its insensitivity to such details.

As seen from Eq. (1) the slope profile of a bended substrate can be represented as a superposition of the characteristic functions weighted with numerical coefficients. These coefficients include all possible inaccuracies of the benders and the substrate manufacturing, assembly, and material properties of the mirror. Assuming linearity of the system all these inaccuracies can be considered as constant parameters inherent to this particular system.

$$f_{1c}^{\,FEA}(x) = \frac{\alpha_2(x) - \alpha_1(x)}{\Delta C_1 \cdot \delta_1} \tag{13}$$

$$f_{2c}^{\,FEA}(x) = \frac{\alpha_3(x) - \alpha_1(x)}{\Delta C_2 \cdot \delta_2}, \tag{14}$$

where the subscript "c" stands for corrected characteristic functions and "δ_1" and "δ_2" are numerical correction coefficients found by fitting the experimental characteristic functions with the FEA calculated ones.

Figure 12 b) shows the differences between measured and corrected FEA calculated characteristic functions. Correction coefficients for the FEA calculated characteristic functions are 0.929 and 0.827 for the upstream and the downstream characteristic functions respectively. The rms errors of these differences are as small as 2.6 nrad/μm and 4.1 nrad/μm for the upstream and the downstream characteristic functions respectively. This uncertainty in the characteristic function calculation may lead to inaccuracy of the mirror setting with just one iteration to tens of microradians over the entire clear aperture starting from an initially flat or slightly pre-bent substrate. In such a case an intermediate slope measurement of the SUT and the second iteration of the mirror setting are essential. However, the overall residual shapes of the characteristic functions' differences most probably can be attributed to not exact coincidence between the actual substrate's shape (see Fig. 2) and its finite element model. More accurate measurements of the actual geometrical parameters of the substrate would let us achieve better coincidence between the actual hardware and its finite element model and avoid unnecessary secondary iterations.

We can measure the characteristic functions on a slightly pre-bent substrate in such a way that the total slope variation would not exceed the measuring range of the LTP. This way, measurement of the characteristic functions consists of three consecutive slope trace measurements made without stitching. At the same time we can simulate by means of FEA the shapes of the finite element model of the substrate for the same parameters of the benders (or for the designed parameters of the benders which correspond to the designed shape of the mirror) and calculate the characteristic functions. Comparing the measured and the FEA-calculated characteristic functions we can find correcting coefficients between the actual hardware and its finite element model. This would let us use FEA-calculated characteristic functions which are smooth and free of the LTP systematic errors and experimental noise.

In the approximation of linearity of the system, which in our case is on the level of 10^{-4}, we can use corrected FEA-calculated characteristic functions for tuning the actual mirror. A simple estimation of accuracy of setting the mirror with just one (the first) iteration starting from slightly pre-bent substrate shows that with a step of 10000 μm possible error of the leaf spring positions will be about 1 μm. This corresponds to the substrate's slope error of 0.6 μrad over the whole clear aperture of the SUT. This value corresponds to the entire range of the characteristic functions multiplied by the value of the leaf spring position error. Such precision of the mirror setting is already on the level of manufacturing accuracy of the substrate. In the case when higher accuracy is needed one more iteration will be sufficient to set the mirror in a closest possible shape to the desired ellipse.

Thereby, measurement of the characteristic functions over the entire clear aperture without stitching and use of the FEA-calculated characteristic functions will considerably save time needed for setting the mirror onto its desired shape without losing precision. Briefly speaking, the time gained in setting a mirror could be multifold and equal to the number of regions over the clear aperture needed to be measured for reliable stitching plus the time for calculation of the stitched slope profiles (or the characteristic functions). The FEA-calculated characteristic functions are free of any kind of experimental noise and systematic errors of the measuring instrument and errors related to the precision of superimposing the measurement regions. Only the final measurement of the slope profile of the SUT, which is set to the desired shape, is needed to be performed with stitching.

Finite element analysis of bended optics may also be very useful for measurement of systematic errors of slope measuring profilers. A manufactured substrate is never ideally shaped, which means that it may not be bent exactly to a shape analytically described by a function. Therefore, comparison of the actual measured SUT's shape with its FEA-calculated one can be done with higher accuracy than benchmarking the measured actual slope against its analytical shape. It allows for a better understanding of systematic errors related to the SUT's quality and to the measuring instrument itself. Comparing the measured slope profile of the actual substrate with the FEA-calculated of the finite element model will allow for better understanding the systematic errors of the measuring instrument. However, in this case one obtains a combination of the systematic errors of the LTP, actual shape of the substrate, and residual slope errors of the substrate polishing.

Direct measurement of LTP systematic errors can be done if an initially flat substrate is measured first in a relaxed unbent condition. In this case the influence of the systematic errors of the LTP optics is not important since the variation of the optical path of the probe beam reflected from the almost flat SUT is much smaller than its width and non-uniformity of the

LTP bulk optics and unevenness of the LTP mirrors are effectively averaged out. However, even when measuring an ideally flat mirror one cannot guarantee that the probe and the reference beams would not be affected by the systematic errors of the LTP optics due to the fact that the optical sensor experiences large wobbling of the order of 2 μrad while moving along the ceramic beam. For better averaging of this error multiple measurements of the mirror with slightly different angular positioning with respect to the LTP must be performed.

Then the substrate is mounted in the bending mechanism and is bent to get an overall slope variation similar to the measuring range of the LTP. The difference between the residual after subtraction of the FEA-calculated slope profile from the measured slope profile of the bent mirror and that of the flat mirror would reveal pure systematic errors of the LTP optics. The systematic error related to wobbling of the LTP optical sensor while moving over the SUT can also be cancelled. It can be achieved by placing the mirror in exactly the same position with respect to the LTP in both cases.

Note that the measured systematic error of the LTP will be of use only in the case if the distance between an SUT and the position of the probe beam on the LTP detector are similar to those as in the case of measurement of this systematic error.

It is useful to note, that the systematic error related to wobbling of the LTP optical sensor could also be measured. This can be obtained by multiple measurements of a flat SUT positioned in various locations along the direction of scanning of the LTP and subtracting the average of these measurements from a single slope measurement. In such a way we can fully characterize our slope measuring profilers and that would substantially improve the accuracy of slope measurements in the OML.

7. CONCLUSIONS

In this work we considered characteristic functions calculated with the help of FEA for force-based and displacement-based boundary conditions applied to the leaf springs of the bendable mirror assembly, and discussed their applicability to the actual hardware. It was shown that the characteristic functions computed by FEA for force-based boundary conditions can be reformulated into ones that correspond to displacement-based boundary conditions without performing additional FEA calculations.

We have applied this FEA-based approach to the bendable mirror M323 of the ALS beamline BL4.0.3 MERLIN, and shown that the system can be considered linear with an accuracy better than 10^{-4}. This level of linearity allows setting the mirror to its desired shape with a precision of 0.6 μrad over the whole clear aperture with just one iteration starting right from an initially relaxed unbent state of the benders.

Contrary to the slope measurement of a curved optic, the differential character of measurement of characteristic functions makes them almost insensitive to systematic errors of slope measuring instruments. Although we have, perhaps, not shown explicitly, we have concluded that in the case when the total slope variation of an optic is larger than that of the measuring instrument the piecewise calculation of characteristic functions with consequent stitching achieves better accuracy than computing characteristic functions from initially stitched slope profiles.

In the case of calculation of characteristic functions some unavoidable minor discrepancy between the finite element model and the actual hardware of the mirror does not matter very much. We have demonstrated that FEA computed characteristic functions of a bendable mirror can be corrected by adding a coefficient of proportionality. This coefficient is obtained by dividing the FEA-calculated characteristic function by the corresponding measured one. The main advantage of this method is the possibility of experimental measurement of the characteristic function of a weakly bent mirror, without stitching for the consequent correction of the FEA calculated one. The use of corrected FEA-calculated characteristic functions can significantly decrease the time needed for setting a highly curved bendable optic to the desired shape, where just one final slope measurement with stitching of a highly curved optic set to its desired shape is needed.

However, to achieve this time savings the actual form of sagittal shaping of the substrate must be carefully measured and embedded in the finite element model. Otherwise, the characteristic functions calculated by FEA and those found experimentally from the actual hardware could have different shapes which may not be corrected by introducing a simple numerical coefficient.

One more useful aspect of measurements of the same substrate in two different states that correspond to initially flat and highly curved shapes can be used for analysis of systematic errors of slope measuring instruments. This work is in progress at the OML.

ACKNOWLEDGEMENTS

The Advanced Light Source is supported by the Director, Office of Science, Office of Basic Energy Sciences, Material Science Division, of the U.S. Department of Energy under Contract No. DE-AC02-05CH11231 at Lawrence Berkeley National Laboratory.

DISCLAIMER

REFERENCES

[1] Erko, A., Idir M., Krist, T., and Michette, A. G., Eds., [Modern Developments in X-ray and Neutron Optics], Springer, Berlin, Germany (2007).

[2] Samoylova, L., Sinn, H., Siewert, F., Mimura, H., Yamauchi, K., and Tschentscher, T., "Requirements on Hard X-ray Grazing Incidence Optics for European XFEL: Analysis and Simulation of Wavefront Transformations," Proc. SPIE 7360, 73600E (2009).

[3] Yuan, S., Church, M., Yashchuk, V. V., Goldberg, K. A., Celestre, R. S., McKinney, W. R., Kirschman, J., Morrison, G., Noll, T., Warwick, T., and Padmore, H. A., "Elliptically Bent X-Ray Mirrors with Active Temperature Stabilization," Hindawi Publishing Corporation, X-Ray Optics and Instrumentation, 2010 (2010).

[4] Siewert, F., Buchheim, J., Boutet, S., Williams, G. J., Montanez, P. A., Krzywinski, J., and Signorato, R., "Ultra-precise characterization of LCLS hard X-ray focusing mirrors by high resolution slope measuring deflectometry," Opt. Express 20(4), 4525-36 (2012).

[5] Kirkpatrick, P. and Baez, A. V., "Formation of Optical Images by X-rays," Journal of the Optical Society of America, 38(9), 766–774 (1948).

[6] Yumoto, H., Mimura, H., Matsuyama, S. Hara, H., Yamamura, K., Sano, Y., Ueno, K., Endo, K., Yabashi, M., Nishino, Y., Tamasaku, K., Ishikawa, T., and Yamauch,i K., "Fabrication of elliptically figured mirror for focusing hard X Rays to size less than 50 nm," Rev. Sci. Instrum., 76, 063708 (2005).

[7] Siewert, F., Lammert, H., Noll, T., Scheleg, T., Zeschke, T., Hänsel, T., Nickel, A., Schindler, A., Grubert B., Schlewitt, C., "Advanced metrology, an essential support for the surface finishing of high performance X-ray optics," Proc. SPIE 5921, 1-11 (2005).

[8] Liu, C., Assoufid L., Conley, R., Macrander, A. T., Ice, G. E., and Tischler, J. Z., "Profile coating and its application for Kirkpatrick-Baez mirrors," Opt. Eng. 42(12),3622–3628 (2003).

[9] Howells, M. R., Cambie, D., Irick, S. C., MacDowell, A. A., Padmore, H. A., Renner, T. R., Rah, S. Y., Sandler, R., "Theory and practice of elliptically bent X-ray mirrors," Opt. Eng. 39(10), 2748–2762 (2000).

[10] McKinney, W. R., Yashchuk, V. V., Goldberg, K. A., Howells, M., Artemiev, N. A., Merthe, D. J., and Yuan, S., "Design optimization of bendable x-ray mirrors," Proc. SPIE 8141, 81410K-1 (2011).

[11] Howells, M. R. and Lunt, D., "Design considerations for adjustable-curvature, high-power, x-ray mirrors based on elastic bending," Opt. Eng. 32(8), 1981—1989 (1993).

[12] McKinney, W. R., Irick, S. C., Kirschman, J. L., MacDowell, A. A., Warwick, T., and Yashchuk, V. V., "New procedures for the adjustment of elliptic ally bent mirrors with the long trace profiler," Proc. SPIE 6704(67040G) (2007).
[13] McKinney, W. R., Irick, S. C., Kirschman, J. L., MacDowell, A. A., Warwick, T., and Yashchuk, V. V., "Optimal tuning and calibration of bendable mirrors with with slope measuring profilers," Opt. Eng. 48(8), 083601 (2009).
[14] Hignette, O., Freund, A., and Chinchio, E., "Incoherent X-ray mirror surface metrology," Proc. SPIE 3152, 188–199 (1997).
[15] Yashchuk, V. V., Barber, S., Domning, E. E., Kirschman, J. L., Morrison, G. Y., Smith, B. V., Siewert, F., Zeschke, T., Geckeler, R., Just, A., "Sub-microradian Surface Slope Metrology with the ALS Developmental Long Trace Profiler," Nucl. Instr. and Meth. A, 616, 212-223 (2010).
[16] Kirschman, J. L., Domning, E. E., McKinney, W. R., Morrison, G. Y., Smith, B. V. and Yashchuk, V. V., "Performance of the upgraded LTP-II at the ALS Optical Metrology laboratory," Proc. SPIE 7077, 70770A (2008).
[17] Kelez, N., Chuang, Y.-D., Smith-Baumann, A., Franck, K., Duarte, R., Lanzara, A., Hasan, M. Z., Dessau, D. S., Chiang, T.C., Shen, Z.-X., Hussain, Z., "Design of an elliptically bent refocus mirror for the MERLIN beamline at the advanced light source," Nucl. Instr. and Meth. A 582, 135–137 (2007).
[18] Reininger, R., Bozek, J., Chuang, Y.-D., Howells, M., Kelez N., Prestemon, S., Marks, S., Warwick, T., Jozwiak, C., Lanzara, A., Hasan, M. Z. and Hussain, Z., "MERLIN — A meV Resolution Beamline at the ALS," AIP Conf. Proc. 879, 509-512 (2006).
[19] http://www.ansys.com/ ANSYS software home page.
[20] See http://www.macrosensors.com/lvdt_tutorial.html for instance.
[21] Merthe, D. J., Yashchuk, V. V., Goldberg, K. A., Kunz, M., Tamura, N., McKinney, W. R, Artemiev, N. A., Celestre, R. S., Morrison, G. Y., Anderson, E., Smith, B. V., Domning, E. E., Padmore, H. A., "Methodology for Optimal In Situ Alignment and Setting of Bendable Optics for Diffraction-Limited Focusing of Soft X-Rays," Proc. SPIE 8501-7, to be published (2012).
[22] Yashchuk, V. V., "Optimal Measurement Strategies for Effective Suppression of Drift Errors," Rev. Sci. Instrum. 80, 115101 (2009).